



Effect of non-erodible particle content on the mechanism of suffusion and the evolution of permeability of sandy soil

Jie Kang¹ · Jie Ren^{1,2} · Songtao Hu² · Hengle Guo¹ · Kaixuan Chen¹ · Ting Zhuang¹ · Shenghao Nan¹ · Jiaheng Sui¹

Received: 3 September 2023 / Accepted: 8 July 2024

© The Author(s), under exclusive licence to Springer-Verlag GmbH Germany, part of Springer Nature 2024

Abstract

Suffusion is a typical type of internal erosion that is an important factor leading to the failure of dams and dikes. In this paper, fine particles are divided into erodible particles and non-erodible particles, and the soil suffusion mechanism is investigated by laboratory tests and CFD_DEM simulations when the content of erodible particles (F_c) and non-erodible particles (F_z) is 15% and 5%, 10% and 10%, and 5% and 15%. The global mean permeability coefficient (k_{av}) and local permeability coefficient (k_{i-j}) were calculated by monitoring the water head in the seepage path of the sample. The results show that with increasing non-erodible particle content, the difficulty of soil suffusion increases gradually. When soil suffusion occurs, the loss of fine particles starts from the seepage outlet area and the influent area, and the non-erodible particles have little influence on the particle loss process in these two areas. After the occurrence of suffusion, the number of weak contact chains is obviously reduced, while the strong contact chains are basically stable. When $F_z = 5\%$ and $F_z = 10\%$, the average permeability coefficient of the soil after suffusion expands to 2.21–1.60 times that of the initial state, and the corresponding values of the CFD_DEM simulation are 2.14–1.86 times.

Keywords CFD_DEM simulation · Laboratory test · Non-erodible particle · Permeability coefficient · Suffusion

1 Introduction

Internal erosion is one of the important reasons for the failure of dams and dikes [21]. According to different occurrence and development mechanisms, internal erosion can be divided into suffusion, backward erosion piping, concentrated leak erosion and contact erosion [9]. Suffusion refers to the migration and loss of fine particles in the soil through pore channels composed of coarse particles under the action of seepage [22], which will change the porosity and permeability of the soil and then lead to changes in the mechanical properties of the soil, causing hidden dangers to engineering operations [2, 18, 23]. The

occurrence and development of suffusion is a long-term process that needs to meet both geometric and hydraulic conditions [1, 9]. The geometric condition refers to that fine particles can migrate through the soil pore channels, which means that the diameter of the soil pore channels needs to be greater than the particle size of the fine particles. The hydraulic condition refers to the need for a large enough seepage force to drive fine particles to migrate in the pore channels of the soil.

The occurrence and development of suffusion are related to the fine particle content, particle size distribution and porosity. Soils prone to suffusion are often referred to as internally unstable soils. At present, some criteria have been established to evaluate the internal stability of the soil mass, such as the fine particle content method, K-L method and nonuniform coefficient method, and the internal stability of the soil mass is determined by the physical parameters of the soil mass [3, 14, 25]. Fine particle content is one of the important criteria for judging the internal stability of soil, and it is generally believed that soil with a fine particle content less than 35% is more prone to internal

✉ Jie Ren
renjie@xaut.edu.cn

¹ State Key Laboratory of Eco-Hydraulics in Northwest Arid Region, Xi'an University of Technology, Xi'an 710048, Shaanxi, China

² Jiangxi Provincial Research Center on Hydraulic Structures, Nanchang 330029, China

erosion [30]. However, the failure types of some soils in practical engineering are not consistent with the theoretical judgement results. Soil prone to suffusion generally has a discontinuous particle size distribution, but slight changes in the initial particle size distribution may also cause soil to change between internal stability and internal instability [26]. Previous studies have shown that evaluating the migration difficulty of fine particles by comparing soil pore diameter with fine particle size is an effective method to determine the possibility of soil suffusion, and this method also takes into account the effects of particle gradation and porosity [16, 37].

The occurrence and development process of suffusion is accompanied by fine particle migration and pore plugging [10, 11, 20]. Fine particles in the soil mass migrate under the drive of seepage, but generally not all of them are lost, and some fine particles will be filtered by the soil pore network, resulting in local pore blockage [38], resulting in an increase in the local hydraulic gradient of the soil mass and a decrease in the permeability coefficient [19, 28, 29]. Pore plugging is caused by the migration of fine particles of different sizes. The stability and scale of pore plugging will affect the development trend of suffusion. Therefore, it is necessary to determine the influence of fine particles of different sizes on the occurrence and development of suffusion.

In recent decades, with the rapid development of computer science, numerical simulation technology has obtained rich research results in the field of geotechnical engineering. The discrete element (DEM), as a discontinuous analysis method, can overcome the shortcomings of finite elements and has unique advantages in analysing the movement of a large number of particles in the process of particle erosion. The coupling method of discrete element (DEM) and computational fluid dynamics (CFD) has good application prospects in the study of soil internal erosion and provides an effective tool for the study of soil internal erosion mechanisms [15, 32, 33].

In this paper, the mechanism of sand suffusion and the evolution law of the permeability coefficient under different fine particle gradation conditions were investigated by laboratory tests and the CFD-DEM coupled numerical simulation method. First, the test equipment and method are introduced, and the evolution process of the global hydraulic gradient, seepage velocity and local hydraulic gradient of the samples with different particle gradations is given. Then, the CFD-DEM coupling method is used to simulate sand suffusion, and the results are compared with laboratory test results. Finally, the evolution process of the soil average permeability coefficient and local permeability coefficient is analysed.

2 Laboratory test of suffusion

2.1 Test equipment

The test equipment includes a water supply system, a model box, a water level monitoring system and a water collection system. Figure 1 is the schematic diagram of the test device, which is described as follows:

- (1) The water supply system includes a water supply tank, a circulating water tank and a water supply pipe. The circulating water tank can keep the liquid level of the water supply tank unchanged, and the water supply pipe connects the water supply tank with the water intake at the bottom of the model tank. The inlet pressure is controlled by adjusting the height of the water supply tank, and the valve is set on the water supply pipe to control the inlet water.
- (2) The model box is made of transparent acrylic plate with a thickness of 10 mm, including a water storage chamber, sand loading room and top baffle, which can clearly observe the test phenomenon. The water storage chamber was 40 cm × 10 cm (length × width × height) and was used to buffer the water flow. A partition board with a round hole is arranged between the water storage chamber and the sand charging chamber. The diameter of the round hole is 5 mm, so that the water can evenly enter the sand charging chamber. The gauze screen is laid on the partition board to prevent the loss of particles. The size of the sand loading room is 40 cm × 10 cm × 30 cm (length × width × height), the water outlet is set at a 30 cm height of the sand loading room, and a baffle with a 10 cm height is set at the top to facilitate the collection of water.
- (3) The water level monitoring system consists of 6 pressure measuring tubes, made of plexiglass with a diameter of 10 mm, evenly distributed on the side of the model box with a spacing of 6.0 cm. The tubes are numbered C1–C6 from bottom to top to obtain the water head data of different positions along the seepage path of the soil sample.
- (4) The water collection system includes a water collection tank and an electronic scale to obtain the amount of water seepage during the test. A gauze screen is set above the collection tank to filter the lost fine sand and ensure the accuracy of the flow data.

2.2 Test protocols and materials

During the occurrence and development of suffusion, the fine particles in the soil migrate and are lost through pore

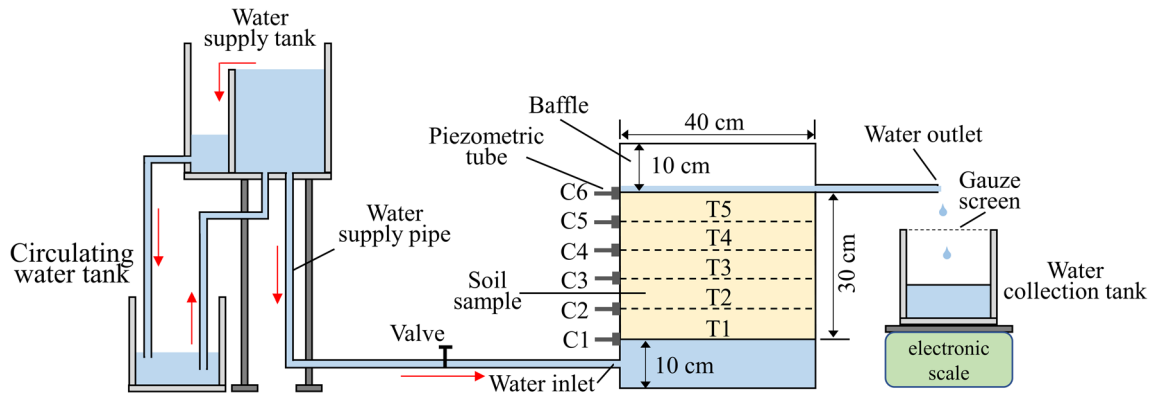


Fig. 1 Schematic of laboratory test system

channels composed of coarse particles under the action of seepage. Previous studies have shown that particles with smaller particle sizes are more likely to be carried out of soil by water flow, while particles with larger particle sizes are less likely to be lost and may even block pore channels. Therefore, taking the average diameter of the soil pore channel R_0 as the dividing point, the fine particles are further divided into erodible particles and non-erodible particles, and the suffusion mechanism and permeability change rule of sand under different erodible particle and non-erodible particle contents are explored. At present, a variety of geometric models have been established to describe the pore characteristics of porous media [18]. The average diameter R_0 of the soil pore channels can be calculated by the following formula [12]:

$$R_0 = 0.63nd_{20} \tag{1}$$

where n is the soil porosity and d_{20} represents that particles smaller than this size account for 20% of the total soil weight of the soil.

The test material is artificially screened sand, including yellow coarse sand and white fine sand, which can clearly observe the particle migration phenomenon during the test. The particle size of the coarse sand ranges from 5 to 10 mm, the density is 2650 kg/m^3 , $d_{20} = 6 \text{ mm}$, and the number is C . It was determined that the minimum porosity of coarse sand was 0.361, and the maximum porosity was 0.417. In this experiment, the porosity of the coarse sand in

each group was controlled at 0.38, the relative density is 69%. According to Eq. (1), the average diameter of the soil pore channel $R_0 = 1.44 \text{ mm}$. Therefore, fine sand with particle sizes ranging from 0.1 to 0.5 mm and 1.5 to 2.0 mm were selected as erodible and non-erodible particles in this test, numbered K and Z in turn.

Current studies have shown that soil with a fine particle content less than 35% is more prone to internal erosion [30]. Therefore, the fine particle mass percentage (defined as R_f) of the sample for this test is set at 20%. The test variable is the proportion of erodible particle content (defined as F_c) and non-erodible particle content (defined as F_z). Three kinds of samples with different particle gradations were configured, and the values of F_c and F_z were 15% and 5%, 10% and 10%, and 5% and 15% and were numbered GP-1, GP-2 and GP-3, respectively. The physical parameters of the three groups of samples are shown in Table 1, and the particle grading curve is shown in Fig. 2.

2.3 Test procedure

The test was conducted in the following steps:

- (1) *Soil sample preparation* First, coarse particles, erodible particles and non-erodible particles were uniformly mixed to prepare the sample, and the mixing ratio was determined according to the values of R_f , F_c and F_z . The volume of coarse particles did

Table 1 Parameters of soil sample

Soil sample	R_f (%)	F_c (%)	F_z (%)	ρ (g/cm ³)	n	d_{10} (mm)	d_{30} (mm)	d_{60} (mm)	Cu	Cc
GP-1	20	15	5	2.59	0.20	0.37	5.63	7.50	2.27	11.42
GP-2	20	10	10	2.59	0.20	0.50	5.63	7.50	15.00	8.45
GP-3	20	5	15	2.59	0.21	1.67	5.63	7.50	4.49	2.53
Coarse sand (C)	–	–	–	2.65	0.38	5.50	6.50	8.00	1.45	0.96
Fine sand (K)	–	–	–	2.35	–	0.14	0.22	0.34	2.43	1.02
Fine sand (Z)	–	–	–	2.32	–	1.55	1.65	1.80	1.16	0.98

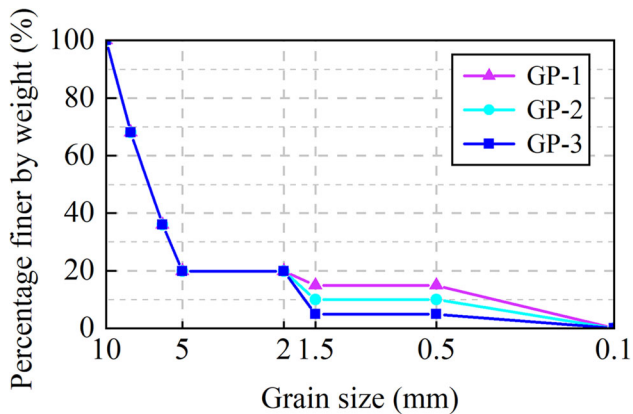


Fig. 2 Particle grading curves of 3 groups of samples

not change when erodible particles and non-erodible particles were added to the coarse particles. This shows that non-erodible particles and erodible particles are free particles located in pores and have nothing to do with coarse skeleton.

- (2) *Sample filling* The sample was filled into the model box in layers, each layer is filled with 6 cm. The sample was prepared by moist tamping. In the process of filling, the weight of each layer sample is calculated by filling volume and soil sample parameters to ensure the uniformity of the sample.
- (3) *Sample saturation* After filling the sample, connect the water supply pipe with the water inlet of the model box, open the valve on the water supply pipe, slowly raise the height of the water supply box, and saturate the sample with water until the top of the sample is almost submerged by water, and then the sample is saturated for more than 24 h. During the saturation process, the air in the sample is discharged through the pressure tube and the surface of the sample.
- (4) *Test process* After the sample is saturated, the height of the water supply tank is raised step by step to start the test, and the height is raised 1.0–2.0 cm each time. After the sample reached stability, the next water level was applied. The criterion for the stability of the sample is that the flow rate of the water outlet and the water level of the pressure measuring pipe remain stable, and there is no obvious particle migration phenomenon. During the test, the water level and flow data of the pressure tube were recorded at intervals of 10 min to analyse the change in soil permeability.
- (5) *Fine sand collection* After the test, the lost fine particles were collected and dried to analyse the loss of soil particles.

3 Test results and analysis

3.1 Erosion of fine particles

Suffusion is a process in which fine soil particles migrate and are lost under the action of seepage. Because of the different migration difficulties of erodible particles and non-erodible particles in soil pores, the occurrence and development trend of suffusion may be affected. Therefore, it is necessary to analyse the particle loss of different samples under the action of seepage, and determine the influence of erodible particles and non-erodible particles on the suffusion of sandy soil.

Figure 3 is a comparison of the upper surfaces of the three samples before and after the test, reflecting the loss of fine particles after the test. Because the surface conditions of the three groups of samples were similar before the test, only the surface image of the GP-1 sample before the test was given, as shown in Fig. 3a. The surface images of the GP-1, GP-2 and GP-3 samples after the test are shown in Fig. 3b–d respectively. It can be seen from the figure that when $F_z = 5\%$ and $F_z = 10\%$, a large number of fine particles in both groups of samples are carried out of the soil by water flow. The image shows that many sand gushers are distributed on the surface of the sample, and the number of sand gushers in the GP-2 sample is relatively large, because the fine particles lost in the GP-1 sample after the test is stopped will cover many sand gushers. In fact, according to the observation of the test phenomenon, the number of sand gushers in the GP-1 sample is greater than that in the GP-2 sample. When $F_z = 15\%$, as shown in Fig. 3d, a small amount of lost fine particles accumulated on the sample surface, without a large-scale fine particle loss phenomenon and obvious sand gusher.

The above results indicate that with increasing non-erodible particle content, the difficulty of fine particle migration and loss gradually increases. Both the GP-1 and GP-2 samples have obvious suffusion, but the loss of fine particles in the GP-2 sample is relatively small, while that in the GP-3 sample does not have obvious suffusion. After the end of the test, no obvious crack, uplift or settlement of the three groups of samples appeared, indicating that the skeleton structure composed of coarse particles of soil was basically stable in the process of seepage.

Figure 4 shows the side image of the GP-3 sample in the test process, which reflects the phenomenon of fine particles migrating and losing under the action of seepage and blocking the soil pore channel. Figure 4 shows that fine particles flow upwards out of the soil under the action of seepage. There is obvious pore blockage on both sides of the image. There are a large number of fine particles in the pore channels composed of coarse particles, but they are

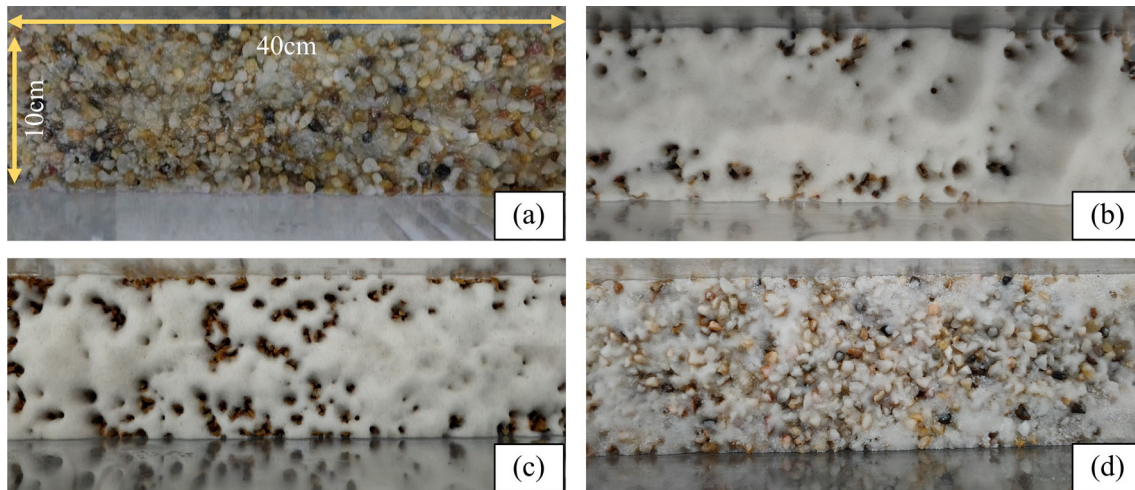


Fig. 3 Surface comparison of soil samples

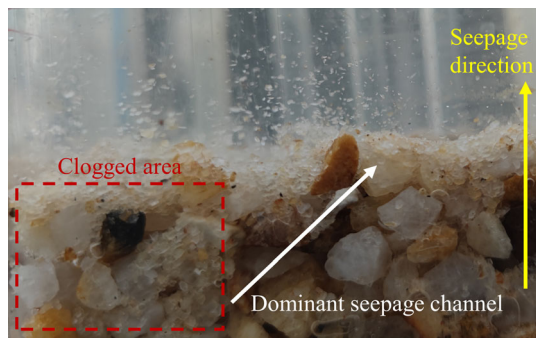


Fig. 4 Migration and loss process of fine particles

not carried out by the water flow, while the fine particles in the pores in the middle of the image are almost all lost, forming a dominant seepage channel. When $F_z = 15\%$, although the non-erodible particles will not cause all the pores to be blocked, it effectively prevents the large-scale migration and loss of fine particles so that no obvious suffusion occurs in the soil sample. It is worth noting that when $F_z = 5\%$ and $F_z = 10\%$, the pores of the soil sample are also blocked, but the number of blocked areas is significantly less than that of the soil sample with $F_z = 15\%$.

3.2 Evolution of seepage velocity and global mean hydraulic gradient

Figure 5 shows the fitting relationship between the seepage velocity (defined as v) and the global mean hydraulic gradient (defined as i) of the three samples. When $F_z = 5\%$ and $F_z = 10\%$, the test process can be divided into a stability stage and an erosion stage. The $v-i$ relationship is basically linear in the stable stage in the early stage of the test, but with the increase in hydraulic gradient, the $v-i$ relationship shows a turning point, indicating that the soil

enters the erosion stage, and the growth rate of v is significantly accelerated compared with the stable stage, indicating that the loss of fine particles leads to the enhancement of soil permeability. At the moment corresponding to the turning point in the $v-i$ relationship, some of the initially blocked particles are detached by the water flow. The i value of the turning point of the $v-i$ relationship can be considered as the critical hydraulic gradient (defined as I) for the sample to undergo suffusion. When $F_z = 5\%$ and $F_z = 10\%$, I is 0.33 and 0.40, respectively, indicating that the difficulty of the sample suffusion increases with increasing non-erodible particle content. This is because the migration of non-erodible particles is more difficult than that of erodible particles, and it will have a blocking effect on the migration and loss of other fine particles. As a result, the fine particles need a larger inlet pressure to be carried out of the soil, and the critical hydraulic gradient of the sample where suffusion occurs is increased.

When $F_z = 15\%$, the $v-i$ relationship turns a turning point when i reaches 0.35. However, contrary to the variation trend of the GP-1 and GP-2 samples, the growth rate of v showed a slightly decreasing trend compared with the early seepage stage, indicating that the sample did not enter the erosion stage when $F_z = 15\%$ and maintained a relatively stable seepage state. This is because the content of non-erodible particles in the GP-3 sample is high. Although fine particles migrate under the action of seepage, only a small amount of fine particles are lost out of the soil, and the remaining fine particles accumulate in the pores of the soil after migration, forming a stronger blocking effect on the seepage of the soil, resulting in a decrease in the permeability of the soil.

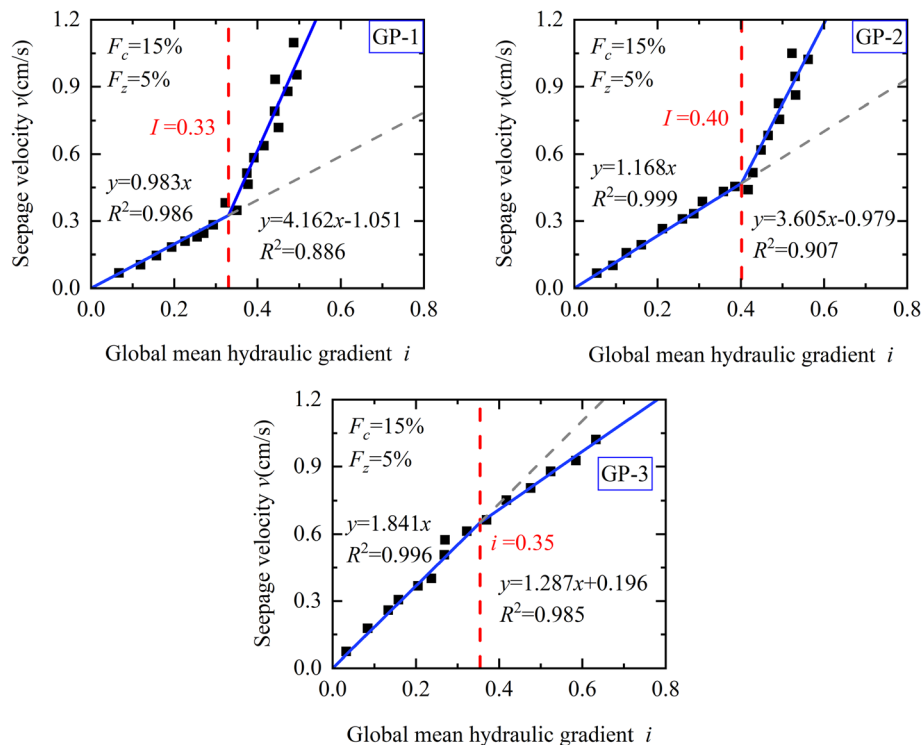


Fig. 5 Relation between seepage velocity and global mean hydraulic gradient

3.3 Evolution of local hydraulic gradients

As shown in Fig. 1, the sample was divided into 5 regions (T1–T5) according to the distribution of pressure tubes, and the local hydraulic gradient between C_m and C_n of the pressure tubes was defined as i_{m-n} . For example, the local hydraulic gradient between C_1 and C_2 is i_{1-2} . Figure 6 shows the relationship between the local hydraulic gradient of the three samples and the test time.

It can be seen from Fig. 6 that the local hydraulic gradient of the soil sample continues to rise on a macro level, which is the result of the continuous increase in inlet pressure. When $F_z = 5\%$ and $F_z = 10\%$, the hydraulic gradients in different regions of the sample are similar in the early stage of the test, and the differences gradually expand after reaching the critical hydraulic gradient for the occurrence of suffusion. i_{1-2} and i_{5-6} basically reach a stable state and are at a relatively low level, while the hydraulic gradients in the middle region of the sample continue to rise. This suggests that particle loss may begin in the seepage outlet region (T5) at the top of the sample and the influent region (T1) at the bottom, resulting in relatively low hydraulic gradients in the T1 and T5 regions. When $F_z = 15\%$, no obvious suffusion occurred in the sample, but compared with $F_z = 5\%$ and $F_z = 10\%$, the evolution trend of i_{1-2} and i_{5-6} did not change significantly, indicating that the non-erodible particle content had little

influence on the fine particle loss process in the T1 and T5 regions. Fig. 3d shows that when $F_z = 15\%$, a small amount of fine particles in the sample are lost, which may be from the seepage outlet area (T5) at the top of the sample.

When fine particle loss occurs in the sample, the particles in the lower part of the sample need to pass through the upper part of the sample to be lost out of the soil. Therefore, the upper region of the sample will face the fine particle supplement effect in the erosion stage, which may also be the reason why i_{1-2} reaches the stable state earlier and is less affected by the non-erodible particle content, because after the loss of fine particles in the T1 region, there will be no new particle supplement to affect the seepage state. i_{5-6} is relatively stable in the erosion stage, indicating that the fine particles in the lower part of the sample have a short retention time after reaching the seepage outlet area (T5) and will quickly be lost from the soil sample, indicating that the fine particles that have migrated are less likely to cause pore blockage in this area.

It can be seen from Fig. 6 that the hydraulic gradient in T2 and T3 regions is significantly higher than the global mean hydraulic gradient. This also indicates that the degree of particle loss in the T2 and T3 regions is relatively low. In addition, the heterogeneity of the local hydraulic gradient increases with increasing non-erodible particle content. When $F_z = 5\%$, i_{3-4} is relatively high. When $F_z = 10\%$, i_{2-3} and i_{3-4} are similar and

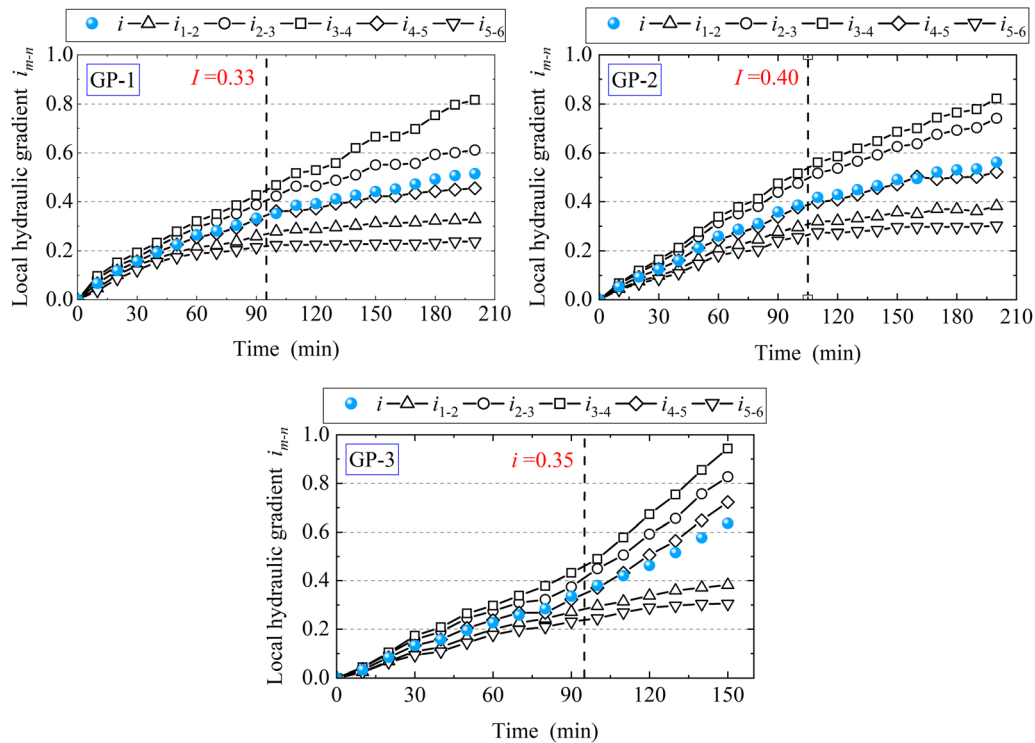


Fig. 6 Evolution of local hydraulic gradient

higher than those in other regions. When $F_z = 15\%$, the local hydraulic gradients showed a trend of polarization, and i_{2-3} , i_{3-4} and i_{4-5} were significantly higher than i_{1-2} and i_{5-6} . This shows that the higher the content of non-erodible particles is, the smaller the erosion range of the sample in space, and the more difficult suffusion failure occurs.

4 Numerical simulation of suffusion

4.1 Construction of the model

The CFD_DEM coupled numerical model with the same grading characteristics as the physical samples was established by particle flow software PFC^{3D}; that is, the contents of coarse particles, non-erodible particles and erodible particles were the same. Numerical models corresponding to soil samples GP-1, GP-2 and GP-3 are numbered SZ1, SZ2 and SZ3 in turn, and model parameters are shown in Table 2. Due to the limitation of computing power, the size of the model was reduced to 40 mm × 40 mm × 80 mm (length × width × height). The particle sizes of coarse particles, non-erodible particles and erodible particles in the numerical model are expressed by the median particle sizes of the test materials in Groups C, Z and K, which are 7.5 mm, 1.75 mm and 0.3 mm, respectively. Figure 7 shows the initial states of the three numerical models. The red particles are coarse particles, the white particles are

Table 2 Numerical model parameters

Computation modules	Parameter types (units)	Values
Solid phase (DEM)	Coarse particle density (kg/m ³)	2650
	Non-erodible particle density (kg/m ³)	2350
	Erodible particle density (kg/m ³)	2320
	Shear stiffness (N/m)	1 × 10 ⁷
	Normal stiffness (N/m)	2.5 × 10 ⁶
	Coefficient of inter-particle friction	0.5
Fluid phase (CFD)	Coefficient of particle–wall friction	0.3
	Fluid density (kg/m ³)	1 × 10 ³
	Dynamic viscosity (pas)	1 × 10 ⁻³
Computational setup	Size of fluid cells (mm)	8
	DEM timestep (s)	5 × 10 ⁻⁷
	CFD timestep (s)	5 × 10 ⁻⁵
	Simulation time (s)	8

non-erodible particles, and the blue particles are erodible particles. The particle numbers of numerical models SZ1, SZ2 and SZ3 are 28,065, 18,896 and 12,503, respectively.

In terms of model boundary conditions, the bottom surface of the model is the pressure inlet, the top surface of the model is the pressure outlet, and other boundary

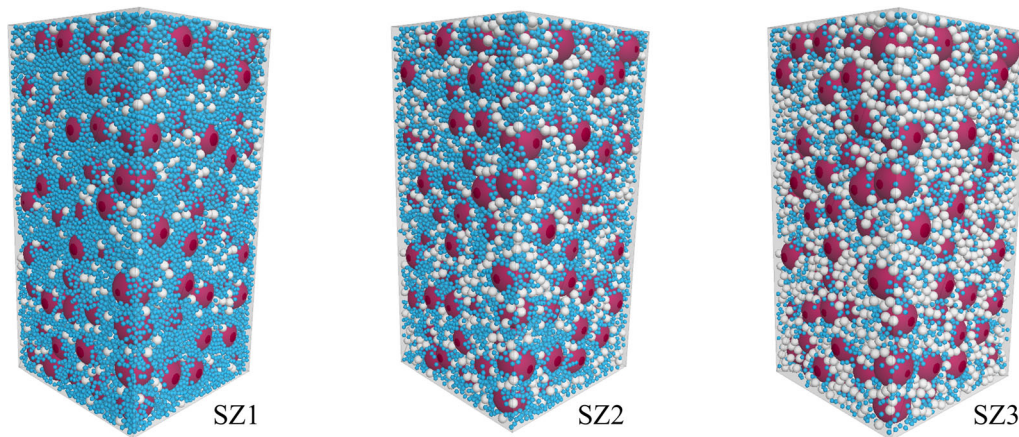


Fig. 7 Schematic diagram of numerical model

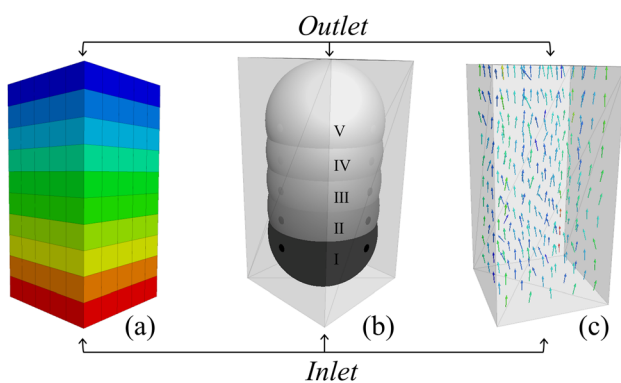


Fig. 8 Model setup: **a** fluid meshing, **b** measurement sphere distribution, **c** direction of water flow

conditions are set as the boundary of the impervious wall. The size of the fluid grid unit is 8×8 mm, and 250 fluid grids are divided, as shown in Fig. 8a. To monitor and record the porosity changes in different regions of the sample during the seepage process, five measuring balls with a diameter of 40 mm were set along the seepage direction, numbered I, II, III, IV and V successively from bottom to top, as shown in Fig. 8b. The water flow direction of the model is from bottom to top, as shown in Fig. 8c.

Table 3 shows the test schemes of the three numerical models. The main test variables are hydraulic gradient and non-erodible particle content. After the particles are balanced, the numerical test of suffusion is carried out, and the equilibrium standard is that the maximum unbalanced force of the particle system is less than 10^{-5} N.

4.2 Model validation

The results of the numerical test and laboratory test were compared to verify the reliability of the model. Figure 9 shows the comparison between the fine particle erosion

Table 3 Numerical simulation scheme

Simulation identity	Soil sample type	Erodible particle content F_c (%)	Non-erodible particle content F_z (%)	Hydraulic gradient i
SZ1-02	SZ1	15s	5	0.2
SZ1-04	SZ1	15	5	0.4
SZ1-06	SZ1	15	5	0.6
SZ2-02	SZ2	10	10	0.2
SZ2-04	SZ2	10	10	0.4
SZ2-06	SZ2	10	10	0.6
SZ3-06	SZ3	5	15	0.6

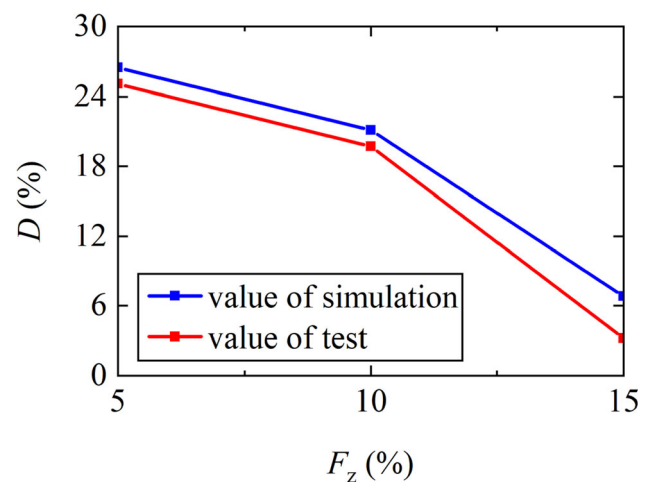


Fig. 9 Comparison of simulation and test results

amount (defined as D) of the three numerical models and the results of laboratory tests under the condition of hydraulic gradient $i = 0.6$. Fine particle erosion amount D is defined as the ratio of the cumulative loss of fine

particles to the initial total amount of fine particles. As shown in Fig. 9, although the model size and hydraulic gradient application process are different, the amount of fine particle erosion in the numerical tests is very close to the laboratory test results. The coupled CFD_DEM method and the simplified particle size distribution can effectively simulate soil suffusion. Both the laboratory test and numerical simulation results show that the fine particle erosion amount decreases with increasing non-erodible particle content.

4.3 The erosion process of fine particles

Figure 10 shows the particle migration and loss process when the non-erodible particle content $F_z = 5\%$ and the hydraulic gradient $i = 0.6$. In the initial state ($t = 0$ s), fine particles are uniformly distributed in the sample, and after the application of seepage, fine particles migrate and are lost through the pore channel between coarse particles. At last ($t = 8$ s), the fine particles were not all lost, the loss was mainly erodible particles, and the coarse particles were in a stable state in the process of seepage.

Figure 11 shows the porosity evolution of tests SZ1-02, SZ1-04 and SZ1-06. When the hydraulic gradient $i = 0.2$, the porosity of each region of the sample increases slightly and slowly. The porosity of measurement sphere V increased the most, from 20.7 to 24.8%, with an increase of 4.1%. The porosity of measurement sphere II increased by 2.3% from 20.2 to 22.5%. After the simulation time $t = 6$ s, the sample porosity tends to be stable. When the hydraulic gradient is low, the particle loss of the sample is small, the loss rate is slow, and the particle loss mainly occurs in the seepage outlet area.

When the hydraulic gradient $i = 0.4$, compared with test SZ1-02, the porosity increase in each region of the sample is significantly increased, and the porosity growth rate is accelerated. The porosity of measurement sphere V increased the most, from 20.7 to 27.7%, with an increase of 7.0%. The porosity increases of measurement spheres I and IV were similar. The porosity of measurement sphere I increased from 20.4 to 25.0%, and the porosity of measurement sphere IV increased from 20.5 to 25.6%, by 4.6% and 5.1%, respectively. The porosity of measurement sphere III increased from 20.5 to 23.8%, an increase of 3.3%. The porosity of measurement sphere II increased by 1.7%. After the simulation time $t = 5$ s, the porosity of the sample tends to be stable. With the increase in the hydraulic gradient, the particle loss of the sample increased significantly, and the particle loss rate in the seepage outlet area accelerated significantly. The main loss range expanded from the seepage outlet area on the upper part of the sample to the two ends of the sample.

When the hydraulic gradient $i = 0.6$, the overall development trend of the sample porosity is similar to that of test SZ1-04, but the growth rate of the porosity in all regions is significantly accelerated. The porosity of measurement sphere V increased by 7.9% from 20.7 to 28.6%. The porosity increases of measurement spheres I, III and IV were close to 5.0%. The increase in porosity of measurement sphere II remained the smallest, with an increase of 1.7%. After the simulation time $t = 4$ s, the sample porosity tends to be stable. With a further increase in the hydraulic gradient, the particle loss rate in each region of the sample is significantly accelerated, and the main loss range extends further from the two ends of the sample to the middle of the sample.

The above research results show that the porosity of each region of the sample presents an upwards trend with increasing hydraulic gradient, and the time required for the porosity to reach stability shortens, indicating that the loss of fine particles gradually increases and the particle loss speed accelerates. When the hydraulic gradient is low, the particle loss of the sample is less, which proves that there is a critical hydraulic gradient in suffusion. The increase in porosity of measurement sphere II in the 3 groups of working conditions is always small, indicating that the particle loss is mainly concentrated at both ends of the sample, and mainly in the seepage outlet area.

4.4 Effect of non-erodible particle content on suffusion

Figure 12 shows the porosity evolution of tests SZ2-02, SZ2-04, SZ2-06 and SZ3-06. For the sample with non-erodible particle content $F_z = 10\%$, when the hydraulic gradient $i = 0.2$, the porosity growth rate of each region of the sample is slow and small. The porosity of measurement spheres I, IV and V increased by approximately 2.0%. The porosity of measurement spheres II and III increased slightly less, approximately 1.0%. When the hydraulic gradient $i = 0.4$, the porosity of the measurement spheres I, IV and V increases by approximately 3.5%. The porosity growth rate of measurement sphere V showed an accelerated trend, indicating that the particle loss rate in this area was accelerated. There was no significant change in the porosity development of measurement spheres II and III. When the hydraulic gradient $i = 0.6$, the development trend of the sample porosity changed obviously. The porosity of measurement spheres I, IV and V all increased by about 7.5%, and the growth rate was accelerated. The porosity of the measurement spheres II and III increased by approximately 4%, but the growth rate did not change significantly. For the sample with non-erodible particle content $F_z = 15\%$, when the hydraulic gradient $i = 0.6$, the

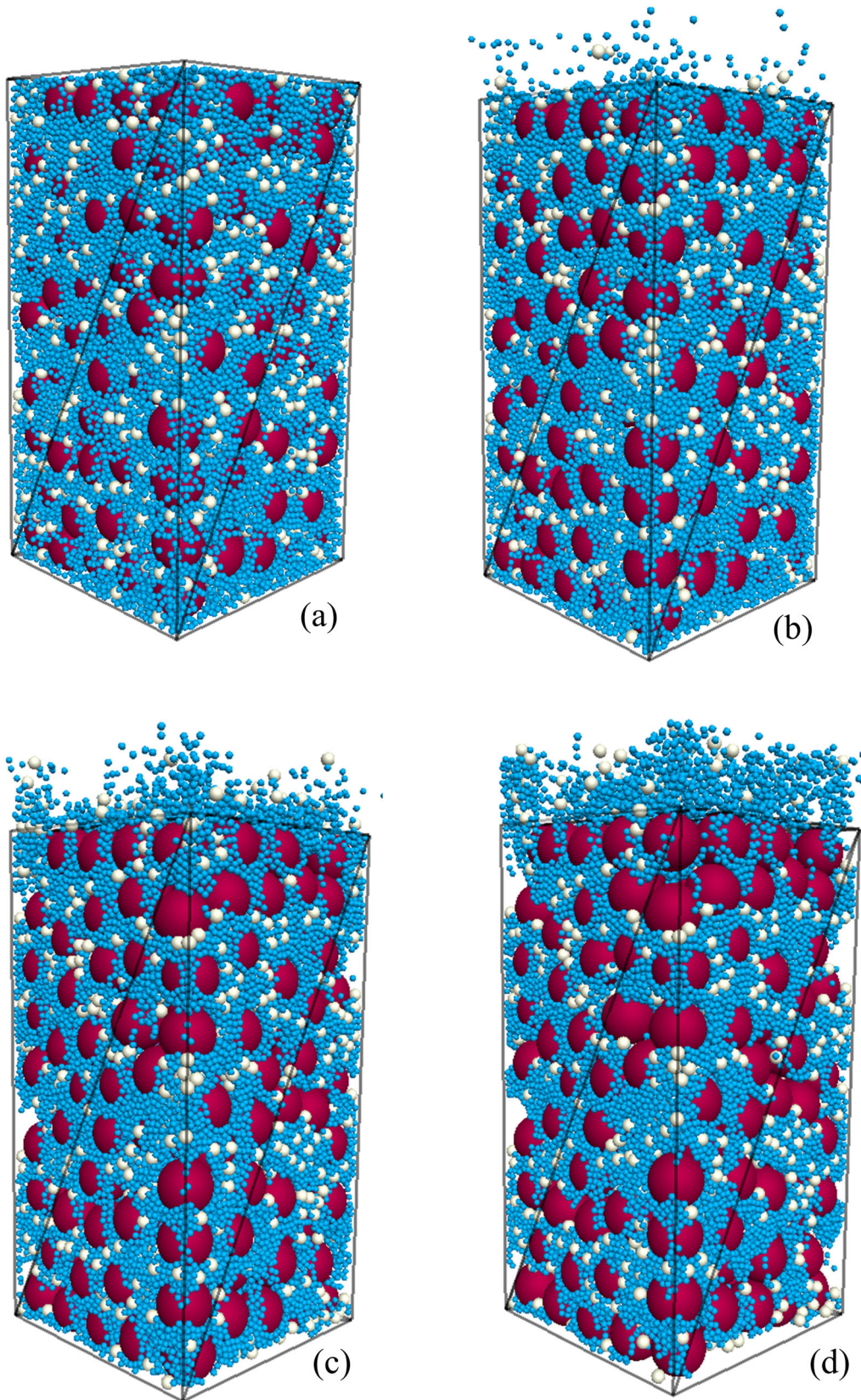


Fig. 10 Migration and loss process of fine particles: a $t = 0$ s; b $t = 1$ s; c $t = 2$ s; d $t = 8$ s

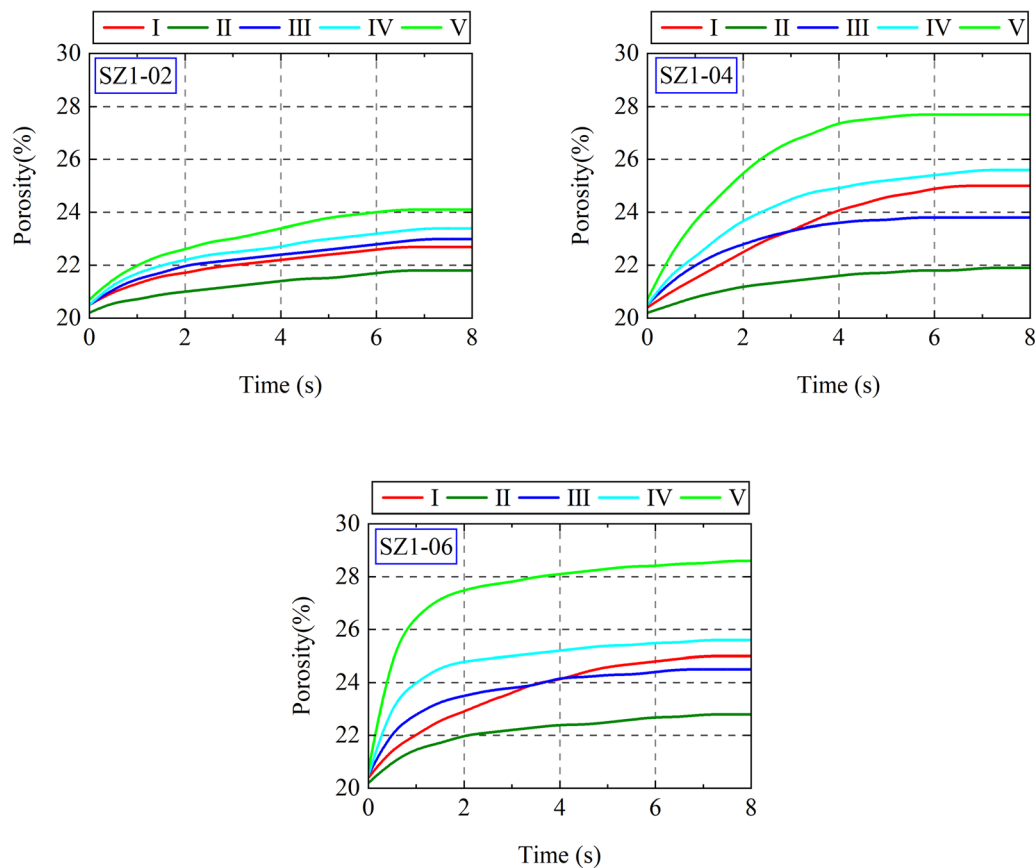


Fig. 11 Evolution of porosity

porosity of each region increases slightly, and then gradually becomes stable.

The above results show that the non-erodible particle content is an important factor affecting the occurrence and development of soil suffusion. Under the same fine particle content, with the increase in non-erodible particle content, the difficulty of soil suffusion gradually increases, which is consistent with the analysis results of laboratory tests. In addition, the time for the SZ2 sample to reach the stable state under different hydraulic gradients is similar, and it does not shorten significantly with increasing inlet pressure. This may be because it is difficult for non-erodible particles to move in the skeleton pores, resulting in the fine particles not being lost out of the soil in a short period of time, and the local migration movement is driven by seepage until a relatively stable blocking structure is formed, thus prolonging the time for the particle system to reach stability.

4.5 Evolution of force chains

Figure 13 shows the evolution of the force chain in the process of seepage of test SZ1-06. The contact force between the particles is represented by the connecting tube,

the diameter of the connecting tube is proportional to the size of the contact force, and the color changes accordingly. As can be seen from Fig. 13, the contact force is mainly transmitted through the coarse particles and forms some strong chains. Due to the contact between particles, weak force chains are formed between fine particles. The development process of the local hydraulic gradient and porosity of the sample shows that the fine particles at both ends of the sample are first lost under the action of seepage, and then gradually expand to the middle of the soil sample. The force chain network of the particle system also reflects the same law of particle migration and loss. In the early stage of seepage, the particle system forms a large number of force chains ($t = 1$ s). With the development of suffusion, the number of weak force chains at both ends of the soil sample began to decrease ($t = 2$ s), indicating that the fine particles at both ends of the soil sample began to migrate and be lost. When the simulation time is $t = 4$ s, the weak force chains at both ends of the sample are further reduced, and the remaining weak force chains are mainly concentrated in the middle of the soil sample. When the simulation time is $t = 8$ s, the continuous seepage leads to the loss of fine particles, and the number of weak force chains is significantly reduced, but there are still some

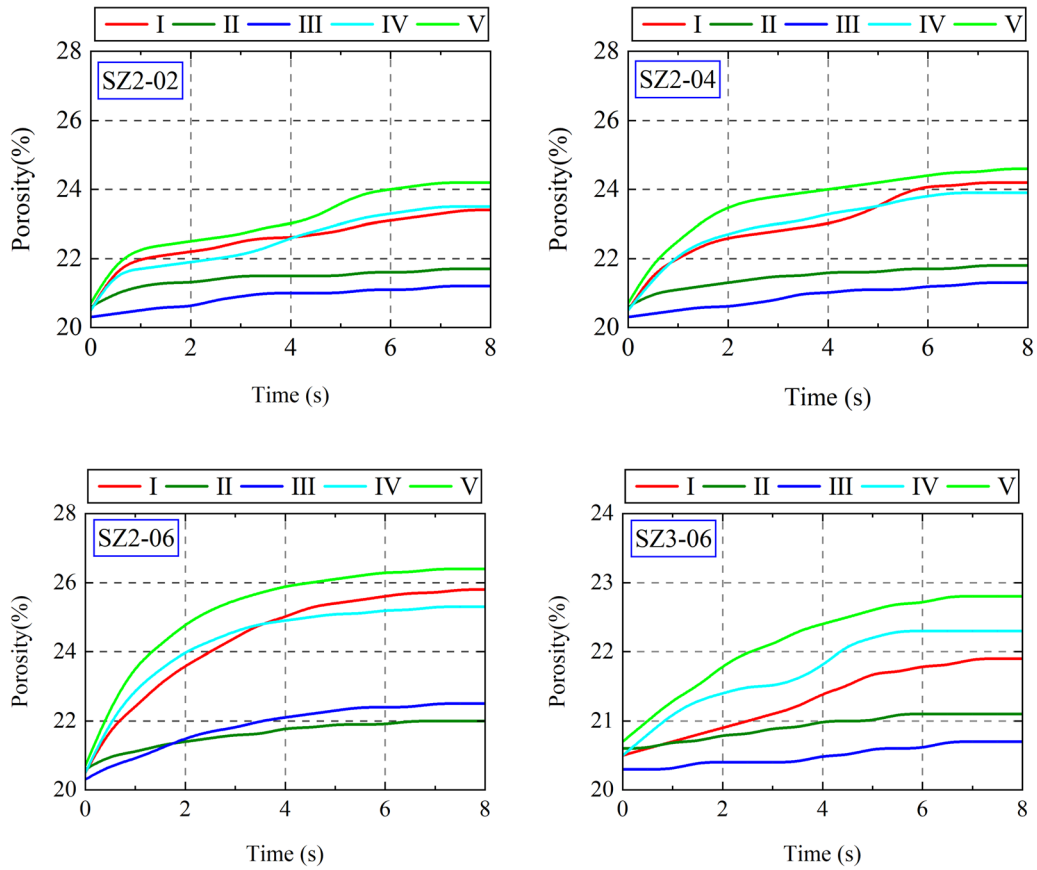


Fig. 12 Evolution of porosity

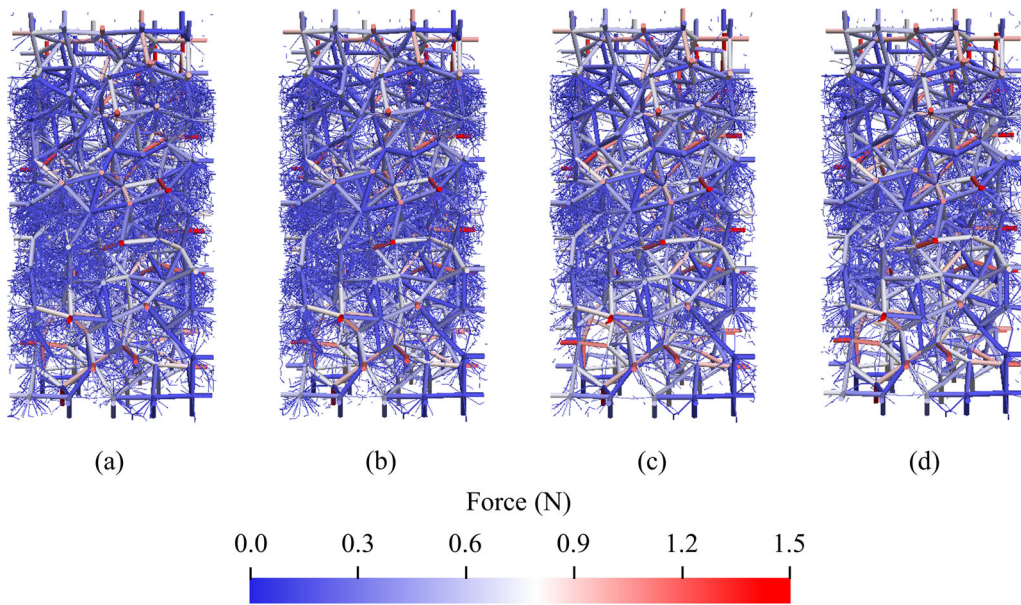


Fig. 13 Evolution process of force chain: a $t = 1$ s; b $t = 2$ s; c $t = 4$ s; d $t = 8$ s

weak force chains in the middle of the soil sample, indicating that the fine particles are not completely lost. During

the seepage process, the strong force chain of the soil sample did not change significantly.

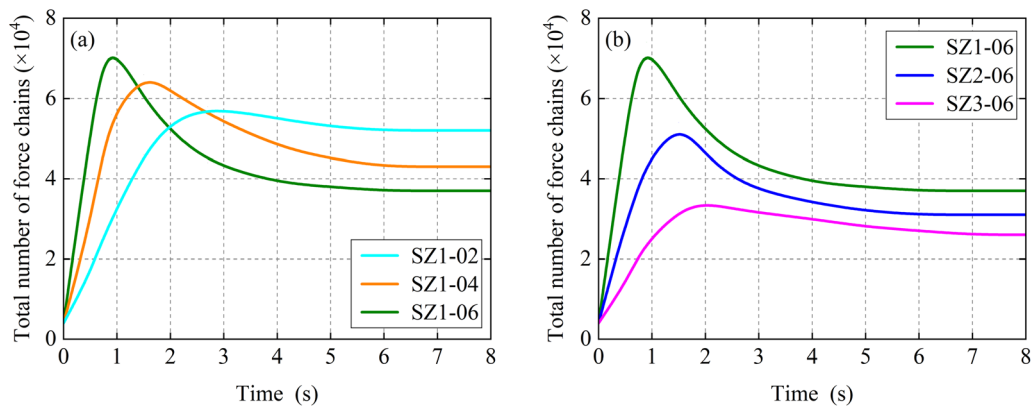


Fig. 14 Evolution of the total number of force chains over time: a $F_z = 5\%$; b $i = 0.6$

Figure 14 shows the evolution process of the total number of force chains with time under different working conditions. For the samples with suffusion (SZ1-04, SZ1-06 and SZ2-06), the evolution process of the total number of force chains can be divided into an increasing stage and a decreasing stage. In the early stage of seepage, particles migrate under the action of seepage and produce a large number of contact forces, and the number of force chains increases significantly. Then, a large number of fine particles are lost under the action of continuous seepage, resulting in a significant reduction in the number of force chains. For the samples without suffusion (SZ1-02 and SZ3-06), the total number of force chains increased significantly in the early stage of seepage. However, due to the low loss of fine particles, the total number of force chains did not decrease significantly in the later period.

The hydraulic gradient and the content of non-erodible particles have obvious influence on the evolution of the total number of force chains. As shown in Fig. 14a, under the condition that the content of non-erodible particles is the same, the decreasing rate of the total number of force chains in the decreasing stage accelerates with the increase of hydraulic gradient. This means that the loss rate of fine particles increases with the increase of hydraulic gradient. In addition, with the increase of hydraulic gradient, the maximum value of the total number of force chains increases. This may be because the larger the hydraulic gradient, the more particles migrate and the more force chains the particles form during migration. As shown in Fig. 14b, under the condition of the same hydraulic gradient, the decreasing rate of the total number of force chains in the decreasing stage slows down with the increase of the content of non-erodible particles. This indicates that non-erodible particles effectively inhibit the loss of fine particles. In addition, with the increase of non-erodible particle content, the maximum value of the total number of force chains showed a decreasing trend. This is mainly

because the initial particle number of the model decreases with the increase of non-erodible particle content.

4.6 Analysis of pore and constriction size distribution of soil skeleton

Constriction is defined as the narrowest part of the channel between the larger pores in the pore network of granular materials and is the main obstacle to be overcome when fine particles migrate through the pores [34, 35]. Therefore, constriction size distribution (CSD) is an important index to evaluate the particle transport capacity of pore channels. At present, the methods for obtaining CSD include experimental, numerical and analytical methods [34]. The pore and constriction size distribution of the sample were obtained based on the Delaunay method [24, 25]. Figure 15 shows the skeleton pore size distribution (PSD) and constriction size distribution (CSD).

As can be seen from Fig. 15, the particle size of erodible particles is significantly smaller than the constriction size of skeleton pores, while the particle size of non-erodible particles is larger than most of the constriction size (76%). This means that the migration of erodible particles in the skeleton pores is less difficult, and it is easy to lose. Non-erodible particles may move within local pores, but it is difficult to migrate between pores. This is the fundamental reason why clogging will gradually dominate as the content of non-erodible particles increases.

Foster et al. [6] suggest classifying the results of filtration tests as “no erosion”, “some erosion” and “continuing erosion”. Under the research conditions of this paper, combined with the research results, it can be concluded that: (1) when the content of non-erodible particles is 5–10%, the sample is in the “some erodible” state; (2) When the content of non-erodible particles reaches 15%, the sample is in the “non-erodible” state. In addition, the local hydraulic gradient and the evolution law of porosity show that the closed constriction is mainly located in the

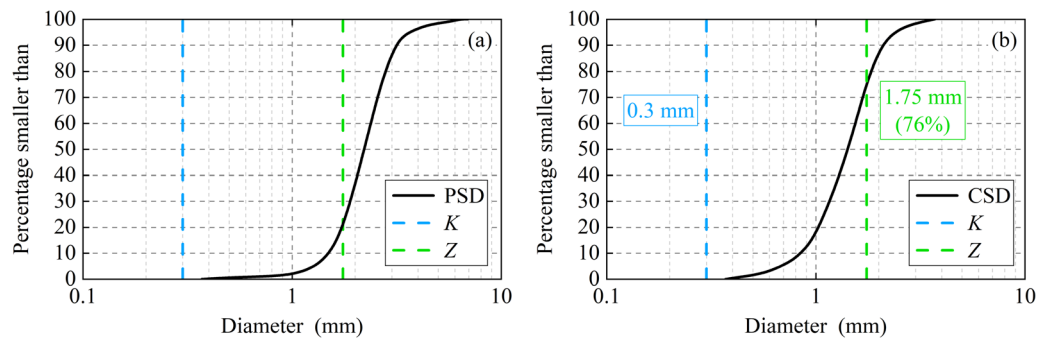


Fig. 15 Pore and constriction size distribution: a PSD; b CSD

middle region of the specimen. It should be noted that the pore system of granular materials is very complex, and the quantification process of pore space will be subjective [31]. The migration of fine particles in pores is affected by many factors [36]. Therefore, the analysis of erosion process based on constriction size distribution and fine particle size distribution is not comprehensive. Pore network model can also deepen the understanding of erosion process [13, 31]. Overall, the effect of the interaction between shrinkage and non-erodible particles on erosion needs further study.

5 The change in the average permeability coefficient

5.1 Evolution of global mean permeability coefficient

The permeability coefficient of sand is calculated according to Darcy's law, and its expression is as follows:

$$k = v/i \quad (2)$$

$$v = Q/S \quad (3)$$

$$i = h/l \quad (4)$$

where: k is the permeability coefficient; v is the average seepage velocity; i is the hydraulic gradient; Q is the seepage rate; S is the area of the seepage cross section; h is the difference in the water head of the pressure measuring pipe; and l is the length of the seepage path.

Figure 16 shows the evolution process of the global mean permeability coefficient (defined as k_{av}) of the three samples in the laboratory test over the test time. When the non-erodible particle content $F_z = 5\%$ and $F_z = 10\%$, k_{av} showed a macroscopic increasing trend, indicating that the permeability of the soil increased after suffusion. Because the migration of fine particles may clog the soil pores, resulting in a decrease in the connectivity of the soil pore channels, k_{av} appears to decrease in stages in the early stage of seepage. When $F_z = 5\%$, k_{av} decreased from 1.02

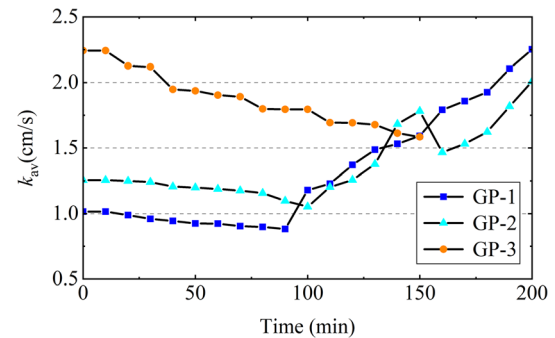


Fig. 16 Evolution of global mean permeability coefficient

to 0.88 cm/s before 90 min, with a decrease of 13.7%. When $F_z = 10\%$, k_{av} decreased from 1.26 to 1.05 cm/s before 100 min, with a decrease of 16.7%. Then, with increasing inlet pressure, continuous seepage causes fine particles to migrate and be lost, and the connectivity of the soil pore channels is strengthened again, resulting in a gradual increase in k_{av} . At the end of the test, the ratio of the final value of k_{av} to the initial value is defined as N_k . When $F_z = 5\%$, k_{av} increases to 2.25 cm/s and $N_k = 2.21$. When $F_z = 10\%$, k_{av} increases to 2.01 cm/s and $N_k = 1.60$. Compared with $F_z = 10\%$, when $F_z = 5\%$, the increase in k_{av} is larger and faster, which means that the loss degree of fine particles is higher and the loss speed is faster. In addition, when $F_z = 10\%$, k_{av} exhibited a fluctuation phenomenon in the late growth stage, indicating that fine particles may temporarily block the soil pores in the subduction stage, but eventually migrate and be lost under continuous seepage. When the non-erodible particle content $F_z = 15\%$, k_{av} showed a continuous decreasing trend from 2.24 to 1.59 cm/s, with a decrease of 29.0%. This is because sample GP-3 did not undergo suffusion, most fine particles were not lost out of the soil after migration, and the pores remained in a state of continuous blockage, resulting in reduced permeability of the soil.

It is worth noting that the higher the content of non-erodible particles is, the stronger the permeability of the soil before the occurrence of suffusion. When $F_z = 15\%$,

the initial k_{av} value is 2.24 cm/s, which is 2.20 times and 1.78 times the initial k_{av} value when $F_z = 5\%$ and $F_z = 10\%$, respectively. When $F_z = 15\%$, the minimum k_{av} is 1.59 cm/s, which is 1.81 times and 1.51 times the minimum k_{av} when $F_z = 5\%$ and $F_z = 10\%$, respectively. Moreover, when $F_z = 15\%$, the minimum k_{av} value is still higher than the initial k_{av} value when $F_z = 5\%$ and $F_z = 10\%$. This indicates that when the content of non-erodible particles reaches a certain critical value, the soil has strong permeability and is not easily damaged by suffusion.

5.2 Comparison between laboratory test and simulation

In the numerical simulation, the soil permeability coefficient [5, 27] is calculated according to the Kozeny–Carman equation, and its expression is as follows:

$$k = \frac{d_{50}^2}{k_c} \frac{n^3}{(1-n)^2} \frac{\rho g}{\mu} \quad (5)$$

where k_c is the Kozeny–Carman coefficient, generally 150 [5], and d_{50} is the equivalent particle size. μ is the motion viscosity coefficient; n is the porosity.

The N_k of the numerical simulation under the hydraulic gradient $i = 0.6$ is calculated. Figure 17 shows the comparison between the laboratory test and numerical simulation of N_k . By comparison, it can be found that when $F_z = 5\%$ and $F_z = 10\%$, the experimental and simulated N_k are very close. When $F_z = 5\%$, the N_k values of the laboratory test and numerical simulation were 2.21 and 2.14, respectively. When $F_z = 10\%$, the N_k of laboratory test and numerical simulation were 1.60 and 1.86, respectively. When $F_z = 15\%$, there is no suffusion in the soil sample, and a large number of fine particles migrate and

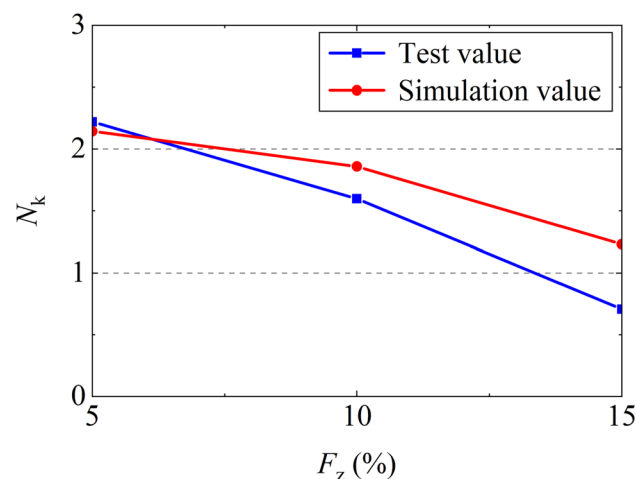


Fig. 17 Comparison between experiment and simulation of N_k

accumulate in the pores, resulting in a decrease in the macroscopic permeability of the soil. Therefore, the test value of N_k is less than 1. In the numerical simulation, the loss of a small number of fine particles leads to a slight increase in the porosity of the sample, so the k_{av} calculated by Kozeny–Carman equation will show a slight increase trend. Therefore, the simulated value of N_k is slightly greater than 1. On a macro level, the growth of the global mean soil permeability coefficient k_{av} of the numerical simulation is close to the results of the laboratory tests, which verifies the reliability of the CFD–DEM coupling model.

5.3 Evolution of the local permeability coefficient

The local permeability coefficient of the sample between the pressure measuring tube Cm–Cn is defined as k_{m-n} . For example, the local permeability coefficient of the sample between C1–C2 of the pressure measuring tube is k_{1-2} . Figure 18 shows the evolution process of the local permeability coefficients of the three samples in the laboratory test with the test time.

When $F_z = 5\%$ and $F_z = 10\%$, the evolution process of the local permeability coefficient can be divided into a stability stage and a growth stage. When $F_z = 5\%$, (1) before the test time reaches 90 min, the local permeability coefficient basically maintains a stable state, and k_{1-2} and k_{5-6} show a slight decreasing trend before 40 min. (2) After the test time reaches 90 min, the local permeability coefficient enters the increasing stage, and the increase amplitude of k_{1-2} and k_{5-6} is large because the fine particles at both ends of the sample are lost to a high degree, resulting in strong local permeability. When $F_z = 10\%$, (1) before the test time reaches 100 min, the local permeability coefficient basically maintains a stable state, and k_{1-2} and k_{5-6} show a slight decreasing trend before 30 min; the decrease is lower than that when $F_z = 5\%$. (2) After the test time reaches 100 min, the local permeability coefficient enters the increasing stage, and there is a fluctuation phenomenon, which may be because the soil pores are briefly blocked. Among them, the fluctuation amplitudes of k_{1-2} and k_{5-6} are larger.

When $F_z = 15\%$, the local permeability coefficient shows a decreasing trend on the macro level. The decrease in k_{1-2} and k_{5-6} was small, and the fluctuation increased in the late stage of the test, which indicated that the fine particles at the two ends of the sample migrated and were lost, resulting in enhanced local permeability. Interestingly, the evolution process of the global mean permeability coefficient k_{av} is similar to that of the permeability coefficient in the middle region of the sample under different non-erodible particle contents.

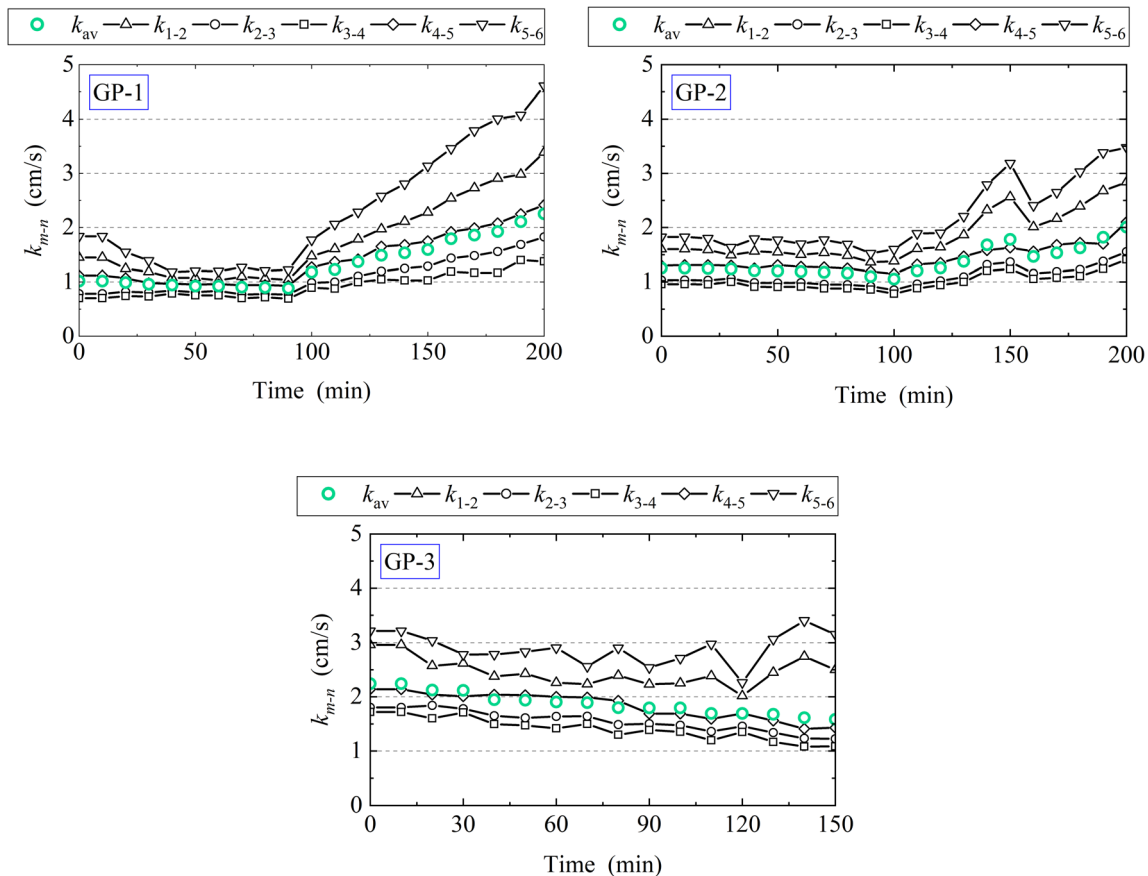


Fig. 18 Evolution of local permeability coefficient

6 Conclusion

Through laboratory tests and CFD_DEM coupled numerical simulation of sand suffusion under vertical seepage conditions, this paper explores the mechanism of sand suffusion and the evolution law of permeability, and mainly draws the following conclusions:

- (1) The occurrence and development process of sand suffusion can be divided into stability stage and an erosion stage. Under the condition of the same fine particle content, the difficulty of soil suffusion increases with increasing non-erodible particle content. The soil changes from suffusion to relative stability under continuous seepage. Therefore, on the basis of considering the fine particle content of soil, it is necessary to classify the fine particles by comparing the pore diameter and the fine particle size to further distinguish the permeability stability of soil.
- (2) Under the effect of vertical seepage, fine particle migration and loss start from the seepage outlet area and the influent area, and the non-erodible particle content has little influence on the particle loss process in these two areas.
- (3) The numerical simulation results based on CFD_DEM coupling show that a large hydraulic gradient will accelerate the loss rate of fine particles. After the loss of fine particles, the weak contact chain in the corresponding region is obviously reduced, while the strong contact chain is basically stable.
- (4) The average permeability coefficient of the soil samples with suffusion decreased first and then increased; the average permeability of the soil samples without suffusion decreased continuously. Before suffusion, the higher the non-erodible particle content of the sample is, the greater the average permeability coefficient. After the occurrence of suffusion, the higher the content of non-erodible particles is, the lower the average permeability coefficient.
- (5) The local soil permeability coefficient calculated by Darcy's law will be affected by other clogged areas. Therefore, a single local permeability coefficient cannot accurately reflect the particle migration and

pore plugging in the corresponding area. In addition, the effect of local plugging on the macroscopic permeability of soil must be considered.

In this paper, the influence of the content of non-erodible particles on the mechanism of suffusion and the evolution law of permeability is discussed, and the inhibition of non-erodible particles on erosion is clarified. Our next work is to quantitatively study the effect of the interaction between non-erodible particles and shrinkage on suffusion from the perspective of micromechanics.

Acknowledgements We thank the precious suggestions by anonymous reviewers and editors, which have greatly helped the improvement of the paper. This work was supported by National Natural Science Foundation of China (Grant No. 52379134), and the Program 2022TD-01 for Shaanxi Provincial Innovative Research Team, and the Fund of Jiangxi Provincial Research Center on Hydraulic Structures (Grant No. 2022SKSG04), and the Open Research Fund of Key Laboratory of Reservoir and Dam Safety Ministry of Water Resources (Grant No. YK323001), and the Research Center on Embankment Safety and Disaster Prevention Engineering Technology of Ministry of Water Resources of China (Grant No. LSDP202304).

Author contributions Jie Kang: Conceptualization, Data curation, Model test, Methodology, writing—review and editing. Jie Ren: Funding acquisition, Formal analysis, Resources, Methodology, Supervision, writing—review and editing. Songtao Hu: Review. Hengle Guo and Kaixuan Chen: Data curation, Writing. Ting Zhuang, Shenghao Nan and Jiaheng Sui: model test, Writing.

Funding National Natural Science Foundation of China, No. 52379134, Jie Ren, Shaanxi Provincial Innovative Research Team, 2022TD-01, Jie Ren, Jiangxi Provincial Research Center on Hydraulic Structures, No. 2022SKSG04, Jie Ren, Key Laboratory of Reservoir and Dam Safety Ministry of Water Resources, No. YK323001, Jie Ren, Research Center on Embankment Safety and Disaster Prevention Engineering Technology of Ministry of Water Resources of China, No. LSDP202304, Jie Ren.

Declarations

Competing interest The authors declare that they have no known competing financial interests or personal relationships that could have appeared to influence the work reported in this paper.

References

- Andreini M, Gardoni P, Pagliara S, Sassu M (2019) Probabilistic models for the erosion rate in embankments and reliability analysis of earth dams. *Reliab Eng Syst Saf* 181:142–155. <https://doi.org/10.1016/j.res.2018.09.023>
- Correia dos Santos RN, Caldeira LMMS, Maranha Das Neves E (2015) Experimental study on crack filling by upstream fills in dams. *Géotechnique* 65(3):218–230. <https://doi.org/10.1680/geot.14.P.198>
- Chang DS, Zhang LM (2013) Extended internal stability criteria for soils under seepage. *Soils Found* 53(4):569–583. <https://doi.org/10.1016/j.sandf.2013.06.008>
- Danka J, Zhang L (2015) Dike failure mechanisms and breaching parameters. *J Geotech Geoenviron Eng* 141(9):04015039. [https://doi.org/10.1061/\(ASCE\)GT.1943-5606.0001335](https://doi.org/10.1061/(ASCE)GT.1943-5606.0001335)
- Ergun S (1952) Fluid flow through packed columns. *Chem Eng Prog* 48:89–94
- Foster M, Fell R (2001) Assessing embankment dam filters that do not satisfy design criteria. *J Geotech Geoenviron Eng* 127:398–407. [https://doi.org/10.1061/\(ASCE\)1090-0241\(2001\)127:5\(398\)](https://doi.org/10.1061/(ASCE)1090-0241(2001)127:5(398))
- Foster M, Fell R, Spannagle M (2000) The statistics of embankment dam failures and accidents. *Can Geotech J* 37(5):1000–1024. <https://doi.org/10.1139/t00-030>
- Fry J (2005) Lessons on internal erosion in embankment dams from failures and physical models. In: *Scour and erosion: proceedings of the 8th international conference on scour and erosion*, (Oxford, UK, 12–15 September 2016), CRC Press, p 41
- Fell R, Wan CF, Cyganiewicz J, Foster M (2003) Time for development of internal erosion and piping in embankment dams. *J Geotech Geoenvironmental Eng* 129:307–314. [https://doi.org/10.1061/\(ASCE\)1090-0241\(2003\)129:4\(307\)](https://doi.org/10.1061/(ASCE)1090-0241(2003)129:4(307))
- Horikoshi K, Takahashi A (2015) Suffusion-induced change in spatial distribution of fine fractions in embankment subjected to seepage flow. *Soils Found* 55(5):1293–1304. <https://doi.org/10.1016/j.sandf.2015.09.027>
- Hu Z, Yida Z, Zhongxuan Y (2019) Suffusion-induced deformation and microstructural change of granular soils: a coupled CFD-DEM study. *Acta Geotech* 14(3):795–814. <https://doi.org/10.1007/s11440-019-00789-8>
- Jie L, Dingsong X (2017) Design principles and guidelines of filters. *Chin J Geotech Eng* 39(4):609–616
- Jang J, Narsilio GA, Santamarina JC (2011) Hydraulic conductivity in spatially varying media: a pore-scale investigation. *Geophys J Int* 184(3):1167–1179. <https://doi.org/10.1111/j.1365-246X.2010.04893.x>
- Kenney T, Lau D (1985) Internal stability of granular filters. *Can Geotech J* 22(2):215–225
- Kawano K, Shire T, O’Sullivan C (2018) Coupled particle-fluid simulations of the initiation of suffusion. *Soils Found* 58(4):972–985. <https://doi.org/10.1016/j.sandf.2018.05.008>
- LiFannin MXJ (2013) Capillary tube model for internal stability of cohesionless soil. *J Geotech Geoenviron Eng* 139(5):831–834. [https://doi.org/10.1061/\(ASCE\)GT.1943-5606.0000790](https://doi.org/10.1061/(ASCE)GT.1943-5606.0000790)
- Lei XQ, Yang ZQ, He SM, Liu EL, Wong H, Li XP (2017) Numerical investigation of rainfall-induced fines migration and its influences on slope stability. *Acta Geotech* 12(6):1431–1446. <https://doi.org/10.1007/s11440-017-0600-y>
- Maroof A, Mahboubi A, Vincens E, Hassani M (2024) A developed capillary tube model for suffusion susceptibility of non-cohesive soils. *B Eng Geol Environ* 83(1):17. <https://doi.org/10.1007/s10064-023-03515-7>
- Marot D, Bendahmane F, Rosquoet F, Alexis A (2009) Internal flow effects on isotropic confined sand-clay mixtures. *Soil Sediment Contam* 18(3):294–306. <https://doi.org/10.1080/15320380902799524>
- Nguyen CD, Benahmed N, Andó E, Sibille L, Philippe P (2019) Experimental investigation of microstructural changes in soils eroded by suffusion using x-ray tomography. *Acta Geotech* 14(3):749–765. <https://doi.org/10.1007/s11440-019-00787-w>
- Özer IE, van Damme M, Jonkman SN (2020) Towards an international levee performance database (ILPD) and its use for macro-scale analysis of levee breaches and failures. *Water* 12(1):119. <https://doi.org/10.3390/w12010119>
- Rochim A, Marot D, Sibille L, Le VT (2017) Effects of hydraulic loading history on suffusion susceptibility of cohesionless soils. *J Geotech Geoenviron Eng* 143(7):04017025. [https://doi.org/10.1061/\(ASCE\)GT.1943-5606.0001673](https://doi.org/10.1061/(ASCE)GT.1943-5606.0001673)

23. Richards KS, Reddy KR (2012) Experimental investigation of initiation of backward erosion piping in soils. *Géotechnique* 62(10):933–942. <https://doi.org/10.1680/geot.11.P.058>
24. Reboul N, Vincens E, Cambou B (2008) A statistical analysis of void size distribution in a simulated narrowly graded packing of spheres. *Granular Matter* 10(6):457–468. <https://doi.org/10.1007/s10035-008-0111-5>
25. Reboul N, Vincens E, Cambou B (2010) A computational procedure to assess the distribution of constriction sizes for an assembly of spheres. *Comput Geotech* 37(1–2):195–206. <https://doi.org/10.1016/j.compgeo.2009.09.002>
26. Skempton AW, Brogan JM (1994) Experiments on piping in sandy gravels. *Géotechnique* 44(3):440–460
27. Schaufler A, Becker C, Steeb H (2013) Infiltration processes in cohesionless soils. *Z Angew Math Mech* 93(2–3):138–146. <https://doi.org/10.1002/zamm.201200047>
28. Sail Y, Marot D, Sibille L, Alexis A (2011) Suffusion tests on cohesionless granular matter: experimental study. *Eur J Environ Civ Eng* 15(5):799–817. <https://doi.org/10.3166/EJECE.15.799-817>
29. Shire T, O’Sullivan C (2013) Micromechanical assessment of an internal stability criterion. *Acta Geotech* 8(1):81–90. <https://doi.org/10.1007/s11440-012-0176-5>
30. Shire T, O’Sullivan C, Hanley K, Fannin R (2014) Fabric and effective stress distribution in internally unstable soils. *J Geotech Geoenviron Eng* 140(12):04014072. [https://doi.org/10.1061/\(ASCE\)GT.1943-5606.0001184](https://doi.org/10.1061/(ASCE)GT.1943-5606.0001184)
31. Shire T, O’Sullivan C (2017) A network model to assess base-filter combinations. *Comput Geotech* 84:117–128. <https://doi.org/10.1016/j.compgeo.2016.11.014>
32. Tao H, Tao J (2017) Quantitative analysis of piping erosion micro-mechanisms with coupled CFD and DEM method. *Acta Geotech* 12(3):573–592. <https://doi.org/10.1007/s11440-016-0516-y>
33. To HD, Torres SAG, Scheuermann A (2015) Primary fabric fraction analysis of granular soils. *Acta Geotech* 10(3):375–387. <https://doi.org/10.1007/s11440-014-0353-9>
34. Vincens E, Witt KJ, Homberg U (2014) Approaches to determine the constriction size distribution for understanding filtration phenomena in granular materials. *Acta Geotech* 10(3):291–303. <https://doi.org/10.1007/s11440-014-0308-1>
35. Wang Y, Dallo YAH (2014) On estimation of the constriction size distribution curve for cohesionless soils. *Eur J Environ Civ En* 18(6):683–698. <https://doi.org/10.1080/19648189.2014.909335>
36. Xiong H, Zhang ZM, Bao XH, Wu H, Yin ZY, Chen XS (2024) Micro-mechanical analysis of particle shape effect on suffusion of gap-graded soils. *Comput Geotech* 165:105925. <https://doi.org/10.1016/j.compgeo.2023.105925>
37. Yousif AH, Wang Y (2016) Determination of controlling constriction size from capillary tube model for internal stability assessment of granular soils. *Soils Found* 56(2):315–320
38. Yang J, Yin ZY, Laouafa F, Hicher PY (2019) Modeling coupled erosion and filtration of fine particles in granular media. *Acta Geotech* 14(6):1615–1627. <https://doi.org/10.1007/s11440-019-00808-8>

Publisher’s Note Springer Nature remains neutral with regard to jurisdictional claims in published maps and institutional affiliations.

Springer Nature or its licensor (e.g. a society or other partner) holds exclusive rights to this article under a publishing agreement with the author(s) or other rightsholder(s); author self-archiving of the accepted manuscript version of this article is solely governed by the terms of such publishing agreement and applicable law.